180° elastic excitation functions for $^{12}C + ^{32}S$, $^{13}C + ^{32}S$, $^{12}C + ^{28}Si$, and $^{13}C + ^{28}Si$ at low bombarding energies

Y-d. Chan
Nuclear Physics Laboratory, University of Washington, Seattle, Washington 98195
and Oak Ridge National Laboratory, Oak Ridge, Tennessee 37830

R. J. Puigh,* W. L. Lynch,† M. Y. Tsang,† and J. G. Cramer
Nuclear Physics Laboratory, University of Washington, Seattle, Washington 98195
(Received 3 August 1981)

We have measured the elastic 180° excitation functions for $^{12}C + ^{32}S$, $^{13}C + ^{32}S$, $^{12}C + ^{28}Si$, and $^{13}C + ^{28}Si$ at low bombarding energies ($V_{CB} \lesssim E_{c.m.} \lesssim 1.8\ V_{CB}$). Gross structures with features resembling those observed at higher energies were observed in the $^{12}C + ^{32}S$ and $^{12}C + ^{28}Si$ systems but not in the other two accompanying reactions. This systematic trend is consistent with compound nucleus level density and channel competition considerations. Conventional optical model potentials with very shallow absorption can generate gross structures comparable to the data in this energy region but over predict the number of peaks.

[NUCLEAR REACTIONS $^{12,13}C(^{32}S,^{32}S)$, $^{12,13}C(^{28}Si,^{28}Si)$, measured elastic $\sigma(E;180°)$; $^{12}C(^{32}S,^{32}S)$ measured elastic $\sigma(\theta)$, $E = 55-99$ MeV; optical model analysis, parity dependent potential.]

I. INTRODUCTION

Since the observation of enhanced backward angle yields in the elastic scattering of $^{16}O + ^{28}Si$ and $^{12}C + ^{28}Si$ by Braun-Munzinger *et al.*[1] and Barrette *et al.*,[2] there has been considerable interest[3–11] in studying the backward scattering phenomena for medium mass heavy-ion systems ($A_p + A_T \lesssim 50$). Most of these measurements have emphasized on energy domains much higher than the Coulomb barrier of the reacting system. In this work we shall report on the result of some 180° elastic excitation function measurements for $^{12}C + ^{32}S$, $^{13}C + 32S$, $^{12}C + ^{28}Si$, and $^{13}C + ^{28}Si$ that concentrate on the lower bombarding energy regions ($V_{CB} \lesssim E_{c.m.} \lesssim 1.8 V_{CB}$). Existing elastic scattering data in the past for this low energy region and comparable systems have been confined mainly to $\theta_{c.m.} \lesssim 140°$, due to experimental difficulties in detecting the backward-scattered low energy projectiles in the conventional light beam on heavy-target configuration. The backward region is, however, expected to be important for optical model studies at low energies, since classically this region corresponds to small impact parameters where the nuclear potential can have strong influence on the otherwise Coulomb dominated scattering amplitude.

In addition to the 180°±4° (c.m.) excitation functions, elastic angular distributions for the $^{12}C + ^{32}S$ system have also been measured at forward angles at $E_{lab}(^{32}S) = 60$, 65, 75, 80, 90, and 99 MeV. Details of the experiment will be discussed in Sec. II. Section III summarizes results of the present measurement. Optical model studies and discussion are presented in Secs. IV to VI.

II. EXPERIMENT

The experiment was performed with the University of Washington FN tandem.

A. The 180° (c.m.) excitation function measurements for $^{12}C + ^{28}Si$, $^{13}C + ^{28}Si$, $^{12}C + ^{32}S$, and $^{13}C + ^{32}S$

The experimental method introduced by Barrette *et al.*[2] was used. The 180° (c.m.) cross sections

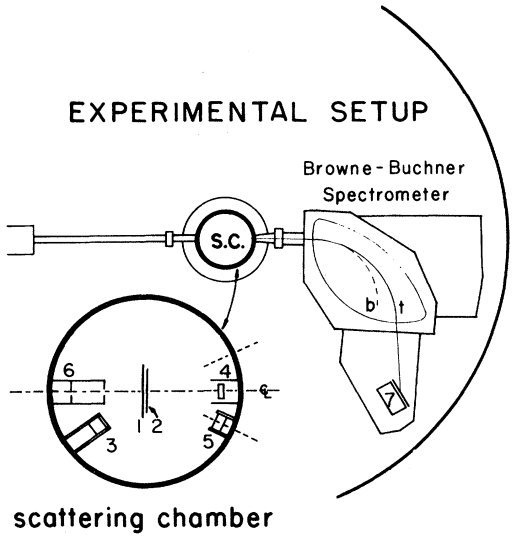

FIG. 1. Experimental setup for the 0°-geometry measurement. 1 = Target wheel; 2 = Ni, Mo foil wheel; 3 = Si monitor (θ_{mon} = 155°); 4 = In-out Faraday cup; 5 = Si Detector (θ=15°); 6 = Beam collimators; 7 = Focal plane detector and mask; t = Target particles; b = Beam particles.

were obtained by detecting the recoiling target particles (^{12}C or ^{13}C) at 0° in the laboratory system. The actual experimental setup is shown in Fig. 1. Beams of ^{28}Si and ^{32}S ions were extracted from a sputter-ion source and accelerated towards a 61 cm diameter scattering chamber. A Browne-Buechner magnetic spectrometer[12] equipped with a position sensitive gas proportional counter at the focal plane was positioned at 0° (lab) with respect to the beam direction to detect the recoiling nuclei. The focal plane counter was basically of the early Rochester design,[13] except that the vertical separation between the cathode and the grid electrodes had been enlarged to 5.1 cm to compensate for the lack of vertical focusing of the spectrometer. As a result of the enlarged geometry the performance of the detector was found to be slightly degraded but still sufficient for the purpose of the present measurement. An intrinsic position resolution of better than 1.8 mm (FWHM) was achieved during all these measurements.

The acceptance angle in the laboratory was $0°\pm2°$ in the scattering plane and was $\sim0.2°$ in the vertical direction. The very small solid angle of the spectrometer, coupled with beam induced background counts in the 0° geometry, placed a practical lower limit on our ability to measure cross sections smaller than 0.1 mb/sr.

Targets were self-supporting isotopic ^{12}C (99%)

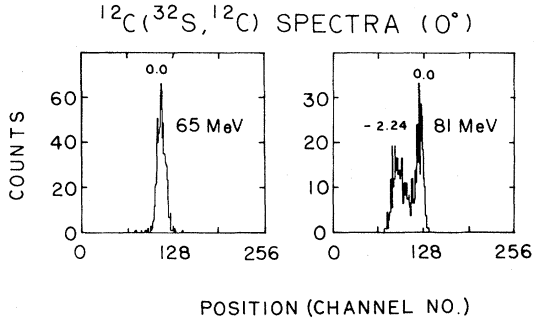

FIG. 2. Sample focal plane spectra obtained at the 0° geometry for the $^{12}C + {}^{32}S$ reaction at $E_L(^{32}S)$ = 65 and 81 MeV.

and ^{13}C (97%) foils of $\sim$50 and $\sim$ 100 $\mu g/cm^2$ in areal density. The 50 $\mu g/cm^2$ targets were used for the lower beam energy measurements. In order to obtain the relative normalization of the data, a thin gold layer had been deposited onto the carbon foils and a Si monitor detector was mounted at θ_{lab} = 155° to detect the Coulomb scattered beam particles from the gold layer. Energy degrading nickel and molybdenum foils of various thickness ($\sim$1.6– 4.0 mg/cm^2) were mounted behind the target foils to remove the accidental degeneracy in magnetic rigidity between the different charge states of the target and beam particles.[2] These foils were mounted on a rotatable mechanism (separated by 0.5 cm from the target) so that different foil thicknesses could be used during the experiment to optimize the removal of degeneracy and the overall energy resolution of the focal plane spectra. Gold and chemically treated silver masks of different thicknesses were also mounted in front of the focal plane detector to stop the residual beam. Two sample focal plane spectra for the $^{12}C + {}^{32}S$ measurement at $E_{lab}(^{32}S)$ = 65 and 81 MeV are shown in Fig. 2 and a monitor spectrum is shown in Fig. 3. The peak corresponding to the

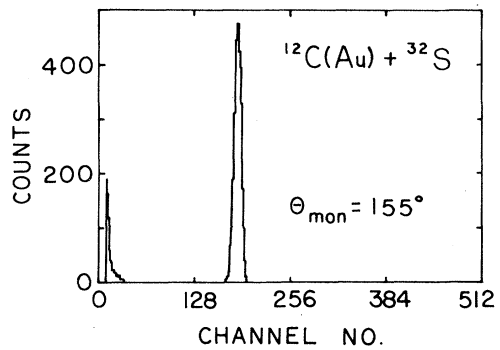

FIG. 3. Monitor spectrum at θ_{lab} = 155° for the $^{12}C(Au) + {}^{32}S$ reaction at $E_{lab}(^{32}S)$ = 60 MeV.

first excited 2^+ state in ^{32}S at 2.24 MeV excitation was strong only at the highest end of the bombarding energy range. The 0° focal plane spectra had an equivalent energy resolution of $\sim$ 1.5 to 2.5 MeV (FWHM) depending on the thickness of the degrading foil and detector mask used. This was sufficient to resolve the $^{32}S(2^+)$ 2.24 MeV and the $^{28}Si(2^+)$ 1.78 MeV states from the ground state peak at the 0° kinematical region.

The elastic cross sections divided by the Rutherford cross section at different energies were obtained by the following relation:

$$\sigma/\sigma_R(E)=K\beta(E)\frac{N}{N_{\text{mon}}},$$

where N is the number of elastic counts in the focal plane spectra and N_{mon} is the number of counts in the elastic gold peak in the monitor spectra. $\beta(E)$ is an energy dependent quantity given by the product of known Jacobian and Rutherford cross section ratios for carbon and gold as well as the detection efficiency of the spectrometer. K is an energy independent systematic constant (comprised of solid angle and target thickness ratios) which in the present case was determined by normalizing σ/σ_R to 1 at the lowest bombarding energy. The normalization energies are below the estimated Coulomb barrier for the individual systems.

The combined detection efficiency (including charge state distribution, corrections due to multiple scattering, and ranging effects in passing through the degrading foils and masks) of the spectrometer system was determined empirically by comparing the scattering of energy-matched ^{12}C beam particles from a thin gold target at θ_{spec} = 15° to a well collimated Si surface barrier counter mounted symmetrically ($-15°$) on the other side of the beam. Such corrections are important in our case, since both the charge state distribution and multiple scattering could vary significantly at low energies. A correction factor of about 5–15% higher than tabulated values[14] for charge state distribution as a function of ion energy was required. The detection efficiency for ^{13}C was assumed to be the same as for ^{12}C.

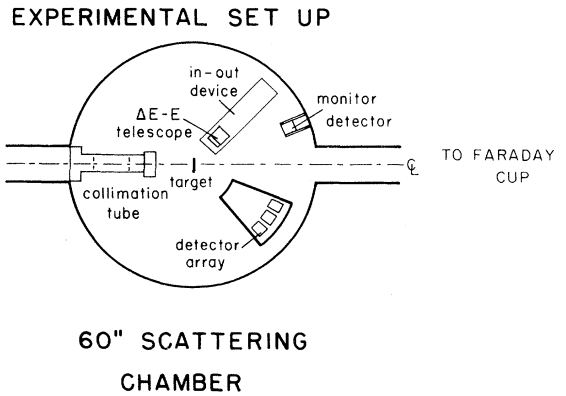

FIG. 4. Experimental setup for the forward angle $^{12}C(^{32}S, ^{32}S)^{12}C$ angular distribution measurement.

B. Forward angle elastic angular distribution measurements for $^{12}C+^{32}S$

In order to supplement the 180° excitation function data, elastic angular distributions for $^{12}C + ^{32}S$ have also been measured at $E_{\text{lab}}(^{32}S)$ = 60, 65, 75, 80, 90, and 99 MeV at the more forward angles. The experimental setup is shown in Fig. 4. Conventional detection methods were used. The targets were thin $^{\text{nat}}C$ foils of $\sim$ 8 μg/cm^2 thick. Three surface barrier detectors mounted on a concentric array were used to detect the scattered particles in singles mode.

At $E_{\text{lab}}(^{32}S)$ = 80 MeV, the angular distribution was extended to more backward angles by detecting the recoiling target particles (^{12}C) with a solid state $\Delta E - E$ telescope mounted on the other side of the beam. The ΔE counter was 9.8 μm thick and the acceptance angle of the telescope in the

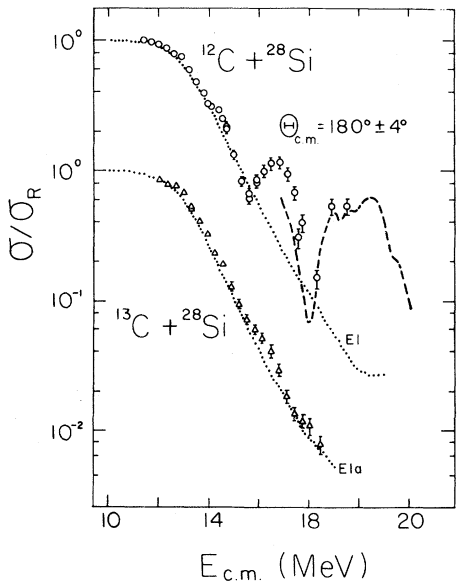

FIG. 5. Elastic 180° excitation functions for $^{12}C + ^{28}Si$ and $^{13}C + ^{28}Si$. The dotted curves are optical model calculations. The dashed curve shows the trend of data from Ref. 1.

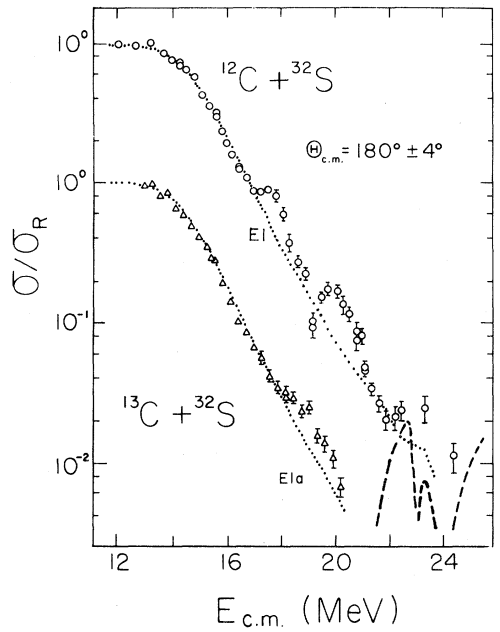

FIG. 6. Elastic 180° excitation functions for $^{12}C + ^{32}S$ and $^{13}C + ^{32}S$. The dotted curves are optical model calculations. The dashed curve shows the smoothed trend of the data on Ref. 6.

scattering plane was 1.5° (lab). The angular distribution data were normalized to the Rutherford cross section at forward angles.

III. RESULTS OF MEASUREMENTS

Results of the 180° excitation function measurements are shown in Figs. 5 and 6. Beam energy loss due to finite target thickness has been corrected for in these plots. Data points overlapping in energy are either taken with different degrading foil and detector mask combinations or from different measurements. Only statistical error bars are indicated. The dotted curves in these figures are optical model calculations to be discussed in Sec. IV.

A. $^{12}C + ^{28}Si$

The bombarding energy range was from $E_{lab}(^{28}Si) = 38$ to 65 MeV. The energy step size at the lower end was comparable to the effective target thickness and sampling effects could be present. A quite distinct structure can be seen at $E_{c.m.} \cong 17$ MeV with an energy width of about 1.5 MeV. The data in the higher energy region has also been measured by Barrette *et al.*[2] and the trend of their data is shown by a dashed curve in Fig. 5. Both measurements agree in the overall behavior of the data in the region where the energy range overlaps. The magnitude of the cross section, however, is about 30% higher in our case. The method of normalization is different for these two measurements and also the acceptance angle is slightly different.

B. $^{13}C + ^{28}Si$

The bombarding energy range was from $E_{lab}(^{28}Si) = 38$ to 58 MeV. There appeared to be a very weak modulation in the data with a period similar to that observed in the $^{12}C + ^{28}Si$ system but the amplitude is much smaller.

C. $^{12}C + ^{32}S$

The bombarding energy range was from $E_{lab}(^{32}S) = 45$ to 90 MeV. The data deviate from the Rutherford cross section at $E_{c.m.} \sim 14$ MeV and decrease exponentially as bombarding energy increases. A shoulder like structure emerges at $E_{c.m.} \cong 17.5$ MeV and a well defined peak can be seen at $E_{c.m.} \cong 20$ MeV. The half-width of the peak is about 1.5 MeV. The same reaction but at the higher end of our bombarding energy range has also been measured by Gelbke *et al.*[6] The general trend of their data is plotted as a dashed curve in Fig. 6. The magnitude of the cross sections in the overlapping region approaches the practical limitation of our detection system as described in Sec. II A. Thus, for $E_{c.m.} > 21$ MeV, our data may have been contaminated with beam induced background counts.

D. $^{13}C + ^{32}S$

The bombarding energy range was from $E_{lab}(^{32}S) = 44$ to 70 MeV. No significant structures are observed as compared with $^{12}C + ^{32}S$ except at $E_{c.m.} \sim 19$ MeV, where the data deviate from a smooth trend.

E. The forward angular distributions for $^{12}C + ^{32}S$

The elastic angular distributions divided by the Rutherford cross section $d\sigma/d\sigma_R(\theta)$ for different

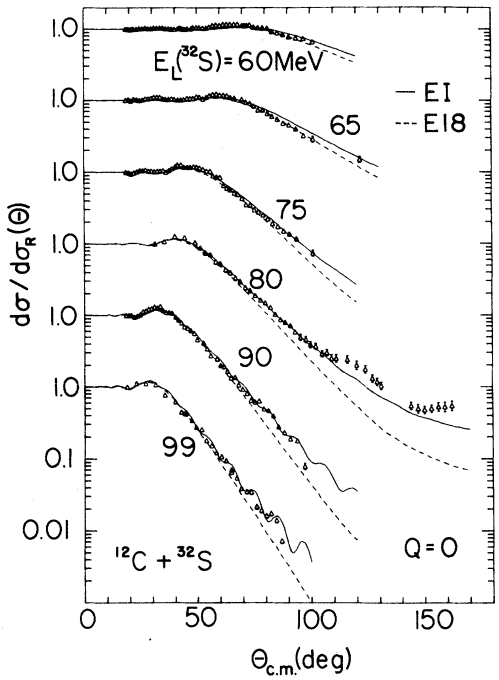

FIG. 7. Forward angle differential cross sections for the elastic scattering of $^{12}C + ^{32}S$. The curves are optical model calculations corresponding to potentials EI (solid curve) and E18 (dashed curve).

bombarding energies are plotted in Fig. 7. The solid and dashed curves are optical model calculations to be discussed in Sec. IV. As is expected for low center of mass energies, the angular distributions at forward angles display little structure except for the data at 90 and 99 MeV, where diffractive patterns are apparent. In addition, large period oscillatory behavior can be observed at backward angles for the 80 MeV angular distribution.

IV. OPTICAL MODEL ANALYSIS

In order to understand what the observed low energy structures in the 180° excitation function may imply, optical model studies have been performed. The $^{12}C + ^{32}S$ system was emphasized, as angular distributions in the low energy region are available.

A. The angular distribution

Conventional six-parameter Woods-Saxon (V, r_V, a_V, W, r_W, and a_W) potentials have been extracted from the experimental data by standard chi-square fitting procedures. To begin with, no energy dependence in V or W was introduced. A global parameter search employing the computer code GENOA was performed on the $E_{lab}(^{32}S) = 60$, 65, 75, 80, 90, and 99 MeV angular distribution sets. The two highest energy sets (90 and 99 MeV) were weighed slightly different from the others so that the numerical search had a higher sensitivity to the diffractive patterns that are apparent in the data. The best-fit result from this search is listed as parameter set EI (abbreviated for energy independent) in Table I. Also listed for comparison is the energy independent six-parameter global potential set $E18$ deduced from the $^{16}O + ^{28}Si$ system.[15] The calculated angular distributions in comparison with experimental data for potential sets EI and $E18$ are shown in Fig. 7. For all of the energies, set EI describes the details of the cross sections reasonably well.

B. The 180° excitation function calculations

The 180° excitation function calculated by the potential set EI for $^{12}C + ^{32}S$ is shown by a dotted curve in Fig. 6. The initial falloff, the magnitude of the cross section, and the general trend of the data can be reproduced, except that no structure in this energy range is predicted. The same potential EI can also describe the averaged trend of the excitation function data for $^{12}C + ^{28}Si$ as shown in Fig. 5.

TABLE I. Potential parameters used in this study. All form factors are Woods-Saxon and the radius parameters are $R_i \equiv r_i(A_p^{1/3} + A_T^{1/3})$.

Set	V_0 (MeV)	r_V (fm)	a_V (fm)	W_0 (MeV)	α	r_W (fm)	a_W (fm)	r_C (fm)
EI	30.00	1.304	0.464	5.00	0.0	1.331	0.399	1.00
EIa	30.00	1.331	0.464	5.00	0.0	1.331	0.399	1.00
E18	10.00	1.350	0.618	23.40	0.0	1.230	0.552	1.00
EED	30.00	1.304	0.464	0.065	0.185	1.331	0.399	1.00

The fact that EI is obtained by fitting the forward angle data and can reproduce the averaged trend of the 180° excitation function is a fairly strong indication that the basic geometry of the real potential in the tail region is being treated correctly. In order to fit the $^{13}C + ^{32}S$ and $^{13}C + ^{28}Si$ 180° excitation function, the real radius r_V has to be slightly increased (EIa in Table I). The calculated results for these two systems are also shown by dotted curves in Figs. 5 and 6.

C. Energy dependent absorption

An attempt to reproduce the structures in the excitation functions was made by introducing energy dependence into the imaginary part of EI. At high incident energies, the energy dependence of the imaginary potential may be weak, as the available reaction phase space at these energies is already large. On the other hand, energy dependence at low bombarding energies can be very important as both the number of compound levels and open reaction channels vary drastically as a function of $E_{c.m.}$. To investigate this, energy dependence has been introduced into the imaginary part of potential EI. Of the different forms of energy dependence that have been tested, the exponentially energy dependent (EED) form $W = W_0 \exp(\alpha E_{c.m.})$ appears to yield the best overall description of the data and is listed in Table I.

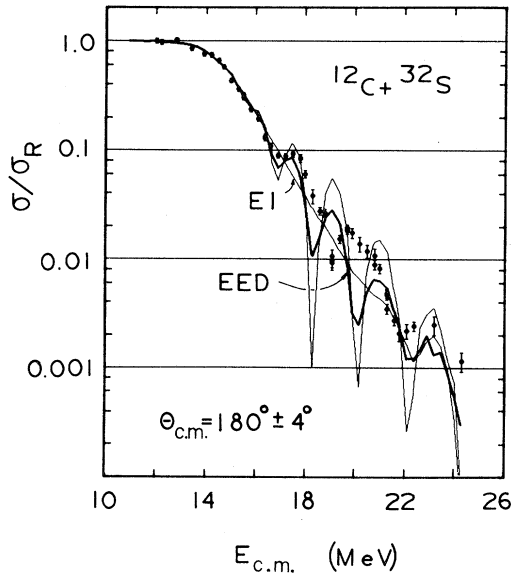

FIG. 8. 180° excitation function for $^{12}C + ^{32}S$ calculated with the exponentially energy-dependent absorption potential EED. The unlabeled thin solid curve corresponds to EED with a reduced absorption strength of $W_0 = 0.055$.

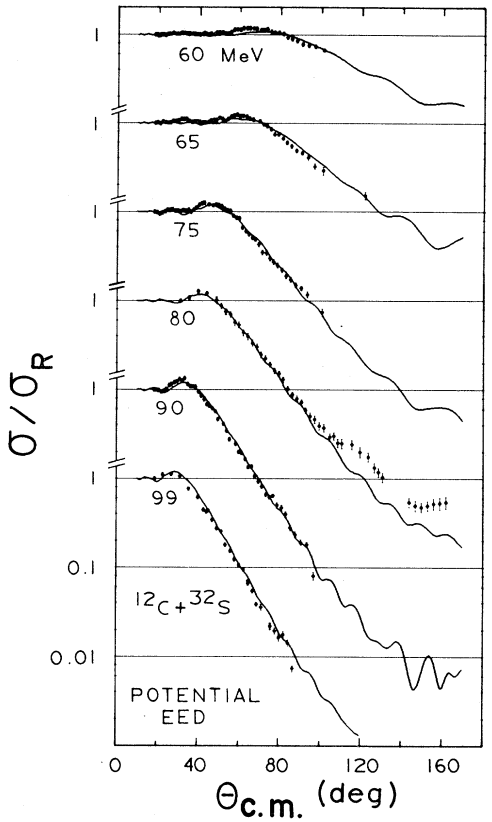

FIG. 9. Forward angle differential cross sections calculated with potential EED for the $^{12}C + ^{32}S$ system.

The 180° excitation function for $^{12}C + ^{32}S$ calculated by this potential is shown by the thick solid curve in Fig. 8. The energy dependent parameters in W for potential EED were adjusted so that the shoulder structure at $E_{c.m.} \sim 17$ MeV could be reproduced. With optimized parameters, the W to V ratio is about 0.05 at this point for the EED set. Structures with width and peak-to-valley ratios comparable to the data can be generated by this potential as shown in Fig. 8. The calculated result, however, does not have the same periodicity as the data. Once the parameters for the real potential are fixed, varying the absorption strength from $W_0 = 0.065$ to 0.05 does not have an appreciable effect on the energy location of the structures (Fig. 8, thin curve). This discrepancy cannot be lifted by minor changes of the parameters of potential set EED.

The forward angle angular distributions calculated by EED are compared with the experimental data in Fig. 9. While the introduction of energy dependence into W (set EED) has drastic effects on

the calculated results for the 180° excitation function (compare Figs. 6 and 8), the forward angular distributions are only slightly affected. This appears to indicate that at low bombarding energies the forward angle cross sections are mainly determined by the real well depth and geometry (e.g., the strong absorption radius) of the potential, and are less sensitive to the detailed absorption of flux inside the nucleus. The backward angle cross section, on the other hand, is very sensitive to the latter.

D. Parity dependent interactions

It has been known that parity dependent interactions play an important role in the elastic scattering of heavy ions in the p shell region where the mass difference between the projectile and target nuclei is small. Both the cluster exchange model[16] and the elastic transfer process[17] provide physical bases for introducing such terms in this mass region. These effects are, however, expected to become less important when heavier mass systems are concerned.

Dehnhard *et al.*[10] have reported success in applying parity dependent potentials to the $^{16}O + ^{28}Si$ system. By introducing a larger potential well depth for the even partial waves, the periodicity of the structures in the 180° excitation function could be well reproduced. To examine the effects of parity dependent potentials in the low $E_{c.m.}$ region similar calculations for the 180° excitation function of $^{12}C + ^{32}S$ have been performed. The potential form we have used is taken from Dehnhard *et al.* and the parameters used are as follows:

$$V_{opt}=[1+(-1)^l C_p](V+iW) ,$$

where C_p is the parity dependent strength parameter given by

$$C_p=P_0\exp(-0.0267E_{c.m.})$$

with $P_0=+0.112$. The Woods-Saxon form factor parameters are

$$V_0=4.0+0.7118E_{c.m.},$$

$$r_V=1.36 \text{ fm}, \quad a_V=0.485 \text{ fm} ,$$

$$W_0=0.02\exp[0.990(E_{c.m.}+11.4)^{1/2}] ,$$

$$r_W=1.35 \text{ fm}, \quad a_W=0.30 \text{ fm},$$

$$r_c=1.0 \text{ fm} .$$

The results of the calculation, corresponding to

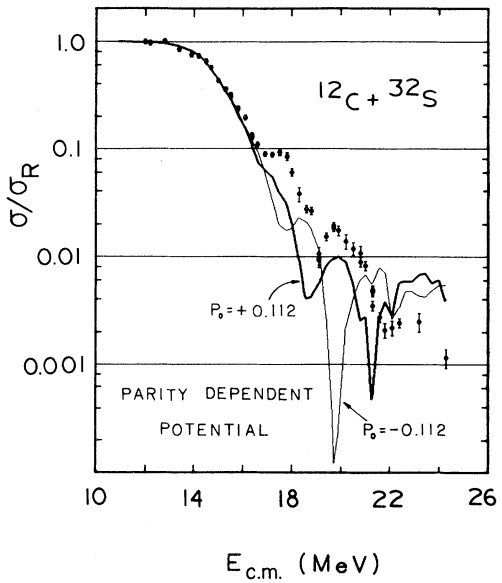

FIG. 10. Parity-dependent potential calculation for the 180° elastic excitation function of $^{12}C + ^{32}S$.

$P_0 = +0.112$ (-0.112), are shown by the thick (thin) curves in Fig. 10. It can be seen that the fit to the periodicity of the peaks is indeed improved. In particular, the present data favors the $P_0>0$ case which corresponds to having a deeper potential for the even-l partial waves. Owing to our limited data base and lack of theoretical guidance on the relevant magnitude of parameters for this system, we have not attempted large parameter space search procedures (with parity dependent potentials) on our data. Nevertheless, it is interesting to note that parity dependent interactions appear to be important over a very wide dynamical range.

V. SYSTEMATIC DEPENDENCE OF THE 180° EXCITATION FUNCTIONS

Our results indicate that the behavior of the 180° excitation functions for $^{13}C + ^{28}Si$ and $^{13}C + ^{32}S$ is much smoother than the other two reactions. This may be due to the differences in absorption strength at comparable energies when the extra neutron is added to ^{12}C to form ^{13}C. To examine this more quantitatively, comparisons have been made in the compound nucleus level densities seen by the grazing partial waves as well as the availability of open direct channels for the $^{13}C + ^{28}Si$ and $^{12}C + ^{28}Si$ systems.

To examine fusion systematics for $^{12}C + ^{28}Si$ and $^{13}C + ^{28}Si$, compound nucleus level densities

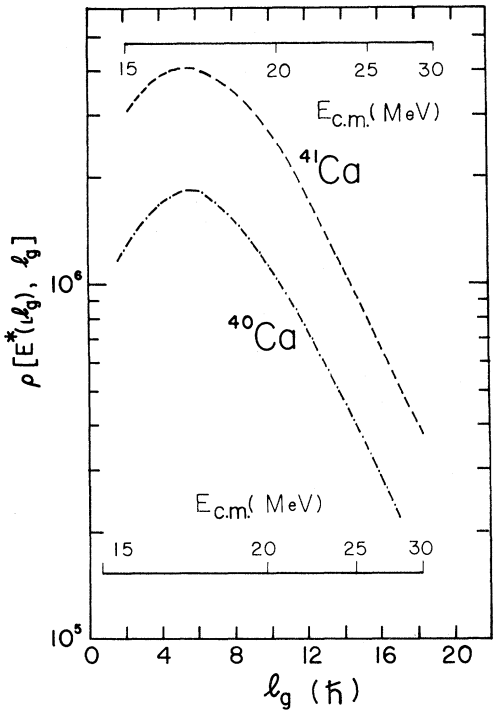

FIG. 11. Comparison of compound nucleus level densities as seen by the grazing partial waves for ^{40}Ca ($^{12}C + ^{28}Si$) and ^{41}Ca ($^{13}C + ^{28}Si$). Also shown are the corresponding center of mass energy scales for $^{12}C + ^{28}Si$ (lower) and $^{13}C + ^{28}Si$ (upper).

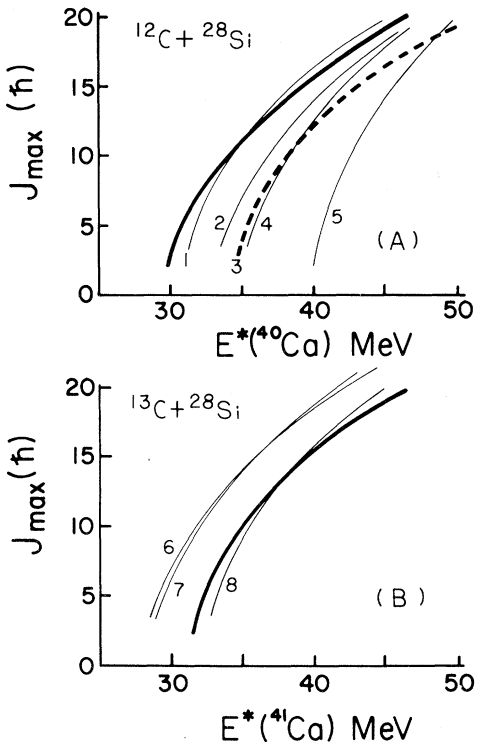

FIG. 12. Comparison of the estimated available maximum angular momentum ($J_{max} = S + l_g$) for various direct exit channels for (a) $^{12}C + ^{28}Si$ and (b) $^{13}C + ^{28}Si$. The entrance channels are denoted by thick solid curves. The other channels are: (1) $^{12}C + ^{28}Si(2^+)$, (2) $^{12}C(2^+) + ^{28}Si$, (3) $^{16}O + ^{24}Mg$ g.s., (4) $^{16}O + ^{24}Mg(2^+)$, (5) $^{16}O(3^-) + ^{24}Mg$, (6) $^{12}C + ^{29}Si$ g.s., (7) $^{12}C + ^{29}Si(\frac{3}{2}^+)$, and (8) $^{13}C + ^{28}Si(2^+)$.

at the grazing angular momenta were compared using the reaction systematic formula of Wilczynski,[18]

$$[l_g(l_g+1)]^{1/2} = kR(1 - E_B/E_{c.m.})^{1/2}$$

$$E_B = Z_p Z_T e^2/R, \quad R = 0.5 + 1.36(A_P^{1/3} + A_T^{1/3}) \text{ fm} .$$

The level density $\rho(E^*,J)$ was calculated by the back-shifted Fermi gas formula with parameters obtained from the systematic formula given by Gilbert and Cameron.[19] The quantity $\rho[E^*(l_g), l_g]$ as a function of l_g is plotted in Fig. 11 for the compound nuclei ^{40}Ca and ^{41}Ca. The level density for the same grazing partial waves in $^{13}C + ^{28}Si$ is about twice as large as in $^{12}C + ^{28}Si$. Similar conclusions can be reached for the $^{12}C + ^{32}S$ and $^{13}C + ^{32}S$ systems. This shows that absorption into the compound nucleus is stronger for $^{13}C + ^{28}Si$ than $^{12}C + ^{28}Si$.

It has been pointed out by Shaw *et al.*[20] that the availability of direct reaction channels capable to remove the large entrance channel angular momentum is also important in explaining the systematic differences of the entrance channel structures in scattering between *p*-shell nuclei. It is interesting to examine if similar arguments could be applied to present mass region.

The comparison of the maximum available angular momenta (J_{max}) for the entrance channel and some of the important exit direct channels for the above two systems is shown in Figs. 12 and 13. Following Shaw *et al.*[20] the J_{max} values have been set equal to the channel spin (S) plus the grazing angular momentum (l_g). It can be seen that for $E^* \lesssim 35$ MeV ($E_{c.m.} \lesssim 20$ MeV), none of the exit direct channels has J_{max} larger than the entrance channel for $^{12}C + ^{28}Si$. On the contrary, as shown in Fig. 12(b), such channels (for instance, the *n* transfer and the $^{25}Mg + ^{16}O$ channels) are always available for $^{13}C + ^{28}Si$ at all bombarding energies. Similar conclusions can also be reached in the comparison of open direct channels of $^{12}C + ^{32}S$ and $^{13}C + ^{32}S$ (Fig. 13). This may justify the application of weakly absorbing potentials in the low energy region for $^{12}C + ^{32}S$ and $^{12}C + ^{28}Si$.

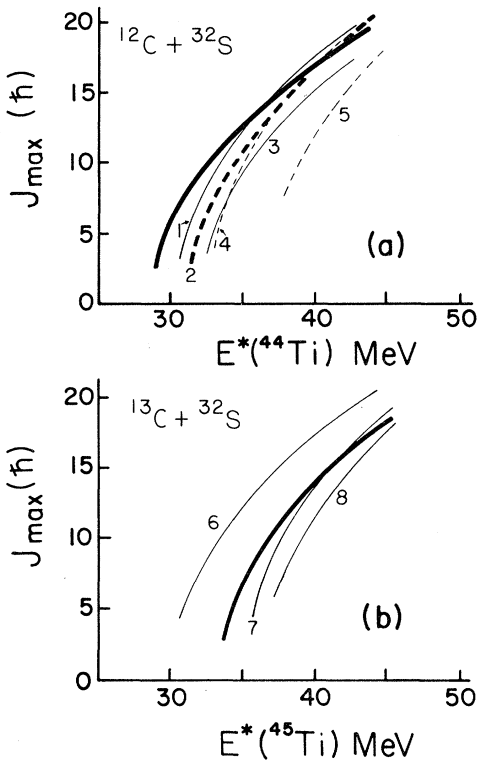

FIG. 13. Same as Fig. 12. but for (a) $^{12}C + ^{32}S$ and (b) $^{13}C + ^{32}S$. The entrance channels are indicated by thick solid curves. The other channels are: (1) $^{12}C + ^{32}S(2^+)$, (2) $^{16}O + ^{28}Si$ g.s., (3) $^{12}C(2^+) + ^{32}S$, (4) $^{16}O + ^{28}Si(2^+)$, (5) $^{16}O(3^-) + ^{28}Si$, (6) $^{12}C + ^{33}S$ g.s., (7) $^{13}C + ^{32}S(2^+)$, and (8) $^{13}C(\frac{5}{2}^+) + ^{32}S$.

VI. CONCLUSION

We have observed gross structures in the 180° elastic excitation functions for $^{12}C + ^{32}S$ and $^{12}C + ^{28}Si$ at rather low bombarding energies. The width and appearance of these structures are quite similar to those that are observed by several other groups[2–7] at higher bombarding energies. Contrary to the ^{12}C data, no comparable structure could be observed in the corresponding $^{13}C + ^{32}S$ and $^{13}C + ^{28}Si$ reactions in the same bombarding energy region suggesting that the gross structures at low bombarding energies are very sensitive to the absorptive properties of the reacting system. We found that the systematic behavior of the data is consistent with simple compound nucleus level density and channel competition considerations.

We have also compared the experimental data with optical model calculations. By using potential parameters extracted from a global fit to the forward angular distribution data, the optical model itself was capable of generating similar structures in the 180° excitation function at low energies, provided that very weak absorption strengths were used. The calculations, however, tend to predict a much shorter periodicity for the recurrence of peaks when compared with the data, a feature which appears to be common for other systems also.[10]

Even though there are still no very convincing physical arguments for introducing parity dependent heavy-ion interactions in this mass region, the quality of fit to the periodicity of the structures could be much improved by using parity-dependent parametrizations such as those suggested by Dehnhard *et al.*[10] The sign of the parity dependent term is such that the nuclear potential is more attractive (deeper) for the even-l partial waves. In the exchange picture, this would imply that the direct and exchange kernels have the same sign.

It should be pointed out that an opposite sign for the parity dependent term ($P_0 < 0$) has been concluded by Kubono *et al.*[21] by fitting simultaneously the 90° and 180° excitation functions for the two lighter systems, $^{28}Si + ^{12}C$ and $^{28}Si + ^{16}O$. This difference, on one hand, may indicate that the extraction of parity-dependent information is potential dependent (especially on the real part); on the other hand, it may also suggest that the parity dependent interaction for heavy ions can have a more complicated systematic dependence. It would be interesting to try and understand this through microscopic wave function model calculations such as those of Baye *et al.*[16] for these systems.

ACKNOWLEDGMENTS

We thank Mr. N. Back and Dr. A. Lazzarini for their help in collecting part of the experimental data. This work was supported in part by the U. S. Department of Energy. Oak Ridge National Laboratory is operated by the Union Carbide Corporation under Contract W-7405-eng-26 with the U. S. Department of Energy.

*Present address: Westinghouse, Hanford, Washington 98352.

†Present address: National Superconducting Cyclotron Laboratory, Michigan State University, East Lansing, Michigan 48824.

[1]P. Braun-Munzinger, G. M. Berkowitz, T. M. Cormier, C. M. Jachcinski, J. W. Harris, J. Barrette, and M. J. LeVine, Phys. Rev. Lett. 38, 944 (1977).

[2]J. Barrette, M. J. LeVine, P. Braun-Munzinger, G. M. Berkowitz, M. Gai, J. W. Harris, and C. M. Jachcinski, Phys. Rev. Lett. 40, 445 (1978).

[3]M. R. Clover, R. M. DeVries, R. Ost, N. Rust, R. N. Cherry, Jr., and H. E. Gove, Phys. Rev. Lett. 40, 1008 (1978); R. Ost, M. R. Clover, R. M. DeVries, B. R. Fulton, H. E. Gove, and N. J. Rust, Phys. Rev. C 19, 740 (1979).

[4]M. Paul, S. J. Sanders, J. Cseh, D. F. Geesaman, W. Henning, D. G. Kovar, C. Olmer, and J. P. Schiffer, Phys. Rev. Lett. 40, 1310 (1978); M. Paul, S. J. Sanders, D. F. Geesaman, W. Henning, D. G. Kovar, C. Olmer, J. P. Schiffer, J. Barrette, and M. J. LeVine, Phys. Rev. C 21, 1802 (1980); S. J. Sanders, M. Paul, J. Cseh, D. F. Geesaman, W. Henning, D. G. Kovar, R. Kozub, C. Olmer, and J. P. Schiffer, *ibid.* 21, 1810 (1980).

[5]S. Kubono, P. D. Bond, C. E. Thorn, and T. R. Renner, Phys. Rev. C. 21, 459 (1980).

[6]C. K. Gelbke, T. C. Awes, U. E. P. Berg, J. Barrette, M. J. LeVine, and P. Braun-Munzinger, Phys. Rev. Lett. 41, 1778 (1978).

[7]S. M. Lee, J. G. Adloff, P. Chevallier, D. Disdier, V. Ranch, and F. Scheibling, Phys. Rev. Lett. 42, 429 (1979).

[8]J. G. Peng, J. V. Maher, M. S. Chiou, M. J. Jordan, F. C. Wang, and M. W. Wu, Phys. Lett. 80B, 35 (1978).

[9]E. H. Auerbach, A. J. Baltz, M. Golin, and S. H. Kahana, in Proceedings of Symposium on Heavy-Ion Elastic Scattering, Rochester, 1977, edited by R. M. DeVries, p. 394.

[10]D. Dehnhard, V. Shkolnik, and M. A. Franey, Phys. Rev. Lett. 40, 1549 (1978).

11 S. Landowne, Phys. Rev. Lett. 42, 633 (1979).

[12]D. K. McDaniel, Ph.D. thesis, University of Washington, 1960.

[13]D. Shapira, R. M. DeVries, H. W. Fulbright, J. Toke, and M. R. Glover, Nucl. Instrum. Methods 129, 123 (1975).

[14]H. D. Betz, Rev. Mod. Phys. 44, 465 (1972).

[15]J. G. Cramer, University of Washington, Nuclear Physics Laboratory Annual Report, 1972; J. G. Cramer, R. M. DeVries, D. A. Goldberg, M. S. Zisman, and C. F. Maguire, Phys. Rev. C 14, 2158 (1976).

[16]D. Baye and P. -H. Heenen, Nucl. Phys. A283, 176 (1977).

[17]W. von Oertzen and H. G. Bohlen, Phys. Rep. 19, 1446 (1975).

[18]J. Wilczynski, Nucl. Phys. A216, 386 (1973).

[19]A. Gilbert and A. G. W. Cameron, Can. J. Phys. 43, 1446 (1965).

[20]R. W. Shaw, Jr., R. Vandenbosch, and M. K. Mehta, Phys. Rev. Lett. 25, 457 (1970).

[21]S. Kubono, P. D. Bond, D. Horn, and C. E. Thorn, Phys. Lett. 84B, 408 (1979).